Addressing the Observability Problem in Batteries: Algorithm Design for Electrode-level Charge and Health Estimation

Sara Sattarzadeh[1], Satadru Dey[1], Andrew Colclasure[2], and Kandler Smith[2]

***Abstract*— From real-time battery estimation viewpoint, weak observability of individual electrode states from terminal voltage measurement is a major barrier. Nevertheless, such electrode-level information can help expand usable energy/power as well as lifespan of the battery cell by enabling electrode-level limit based battery control. Motivated by these promising improvements, we present a real-time framework for estimating charge and health of individual electrodes. Essentially, the weak observability of the electrodes is addressed by decomposing the overall estimation problem into two sub-estimators that work in a cascaded manner to provide charge and health information for individual electrodes. The performance of the proposed scheme is illustrated by using an experimentally identified battery model that considers essential nonlinearities in electrodes' Open Circuit Potential (OCP) functions and resistances as well as dominant Solid Electrolyte Interphase (SEI) aging mechanism. Simulation case studies are presented based on this identified model which validate the effectiveness of the proposed framework.**

I. INTRODUCTION

Although Lithium-ion Batteries (LIBs) are being considered to be promising for many applications, safety remains a key issue for LIBs. Real-time information on battery electrode-level quantities can be beneficial in improving safety as well as performance. From estimation theory viewpoint, the major obstacle in designing an electrode-level estimation scheme arises from weak observability [1], [2]. Nevertheless, such electrode-level information can help expand usable energy/power as well as lifespan of the battery cell by enabling electrode-level limit based battery control [3], [4].

Battery cell-level estimation problems have been widely explored in literature [1], [2]. Very few studies have been conducted on battery electrode-level State-of-Charge (SOC) and State-of-Health (SOH) estimation problems. For example, the algorithms in [3], [5], [6], estimate Lithium concentration (equivalent to electrode SOC) in individual electrodes assuming some of the capacity-related parameters such as total moles of Lithium and electrode's volume fraction are known and constant. However, this assumption may not be practical as these parameters change due to the battery aging. In [7], an algorithm is proposed for individual electrode's Lithium concentration estimation under the assumption that perfect open-loop model is available. However, assumption of such model knowledge may be impractical in real-world applications. A parameter identification based approach is presented in [8] to estimate individual electrode's capacity and utilization window. Although this approach provides individual electrode's SOH information via capacity estimation, it does not provide real-time information of individual electrode's SOC.

To address the aforementioned limitations, we have proposed an estimation algorithm in our previous work [4] that simultaneously estimates individual electrode's SOC and SOH without making the aforementioned limiting assumptions. However, the work in [4] is based on a simplified battery model which does not consider (i) dominant aging factor of Solid Electrolyte Interphase (SEI) growth, and (ii) nonlinear dependence of electrode resistances on electrode SOC. Note that SEI aging and nonlinear resistances are integral part of battery physical dynamics and degradation, and it is crucial to accommodate them within the model-based estimation framework. In this work, we extend the approach proposed in [4] by designing an electrode-level SOC-SOH estimation algorithm considering electrode-level dynamics, SEI growth aging model and nonlinearity in electrode resistances. Specifically, we propose a terminal voltage feedback-based closed-loop cascaded estimation algorithm to address the weak observability issue regarding electrode-level estimation. We also analyze the mathematical properties of the proposed scheme using Lyapnov's stability theory. Finally, the effectiveness of the proposed method is evaluated by using an experimentally identified battery model.

The organization of this paper is as follows. Section II formulate the model of individual battery electrodes. Section III presents the electrode-level estimation algorithm. Section IV describes the model identification from experimental data. Sections V presents the simulation results and discussions while Section VI presents conclusion.

II. BATTERY ELECTRODE MODEL

In this section, we discuss the battery model adopted for this work. The stoichiometry dynamics of each electrode is modelled as follows:

$$\dot{y}(t) = \frac{I(t)}{Q_p},\ \dot{x}(t) = \frac{-I(t)}{Q_n} - \frac{\dot{Q}_{SEI}(t)}{Q_n}, \tag{1}$$

where $x \in [0,1]$ and $y \in [0,1]$ represent the dimensionless stoichiometries of negative and positive electrodes, respec-

*This work was supported in part by the National Renewable Energy Laboratory via subcontract no. XCE-9-92129-01 (under prime contract no. DE-AC36-08GO28308), and National Science Foundation under award no. 1908560.

[1]S. Sattarzadeh and S. Dey are with the Department of Electrical Engineering, University of Colorado Denver, CO 80204, USA {sara.sattarzadeh, satadru.dey}@ucdenver.edu.

[2]A. Colclasure and K. Smith are with the National Renewable Energy Lab, Golden, CO 80401, USA. {andrew.colclasure, kandler.smith}@nrel.gov.

tively; I in $Ampere$ (A) is the battery cell current with $I > 0$ representing full cell discharge operation; Q_p and Q_n are the capacities of positive and negative electrodes in $Ampere - seconds$ (A-sec), respectively; Q_{SEI} is the lithium inventory in $Ampere-seconds$ (A-sec) due to Solid Electrolyte Interphase (SEI) growth. Furthermore, we model the dynamics of Q_{SEI} as follows:

$$\dot{Q}_{SEI}(t) = \frac{k_{SEI}^2}{2Q_{SEI}(t)}, \tag{2}$$

where the parameter $k_{SEI} > 0$ characterizes the time scale of Lithium loss due to SEI. Finally, the terminal voltage of the battery cell is given by:

$$V_t(t) = f_p(y) - f_n(x) - I(t)\big(R_p(y) + R_n(x)\big), \tag{3}$$

where $f_p(.)$ and $f_n(.)$ are the Open Circuit Potential (OCP) functions of the positive and negative electrodes, respectively, expressed in $Volts$; R_p and R_n are the internal resistances of positive and negative electrodes, respectively, expressed in Ω. Note that the OCP functions and resistances are nonlinear functions of individual electrode stoichiometries.

III. ONLINE ESTIMATION ALGORITHM

In this section, we describe the online estimation algorithm. The objective of the estimation algorithm is to estimate the available charge and health of the positive and negative electrodes. In order to achieve such goal, we estimate (i) stoichiometries x and y which capture the SOC state of each electrode, and (ii) Q_p, Q_n, and Q_{SEI} which capture the SOH states of the electrodes. A schematic of the estimation algorithm is shown in Fig. 1. Note that the algorithm uses filtered terminal voltage as measured feedback which is commonly available in commercial battery cells. The purpose of the filters is to reduce the effect of measurement noise. Furthermore, the estimation algorithm consists of two sub-estimators working in cascade. The first sub-estimator is called *Positive Electrode Estimator* which estimates positive electrode's SOC and SOH (i.e. y and Q_p) based on filtered terminal voltage feedback. The second sub-estimator is *Negative Electrode Estimator* which receives filtered terminal voltage feedback and estimated y from the *Positive Electrode Estimator*, and subsequently estimates negative electrode's SOC and SOH (i.e. x, Q_n and Q_{SEI}).

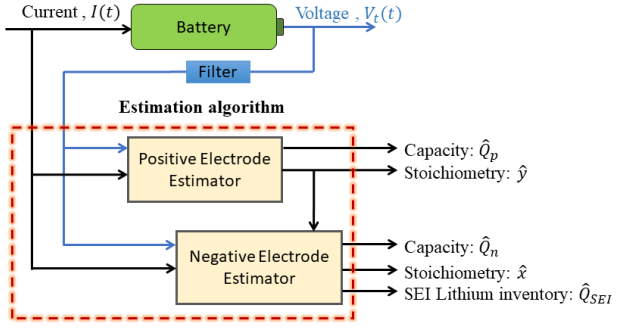

Fig. 1. On-line estimation algorithm for electrode-level SOC (stoichiometries x; y) and SOH (capacities Q_p, Q_n) estimation.

As mentioned before, a major problem in battery estimation lies in weak observability of the electrode states from terminal voltage. That is, the dynamic system states x and y in (1) are not observable from the output voltage V_t. To address such issue, we decouple the original system (1) into two subsystems: one consisting of positive electrode dynamics (the first equation in (1)) and the other consisting of negative electrode dynamics (the second equation in (1)). As will be shown next, we design *Positive Electrode Estimator* and *Negative Electrode Estimator* based on these two sub-systems. Furthermore, while using the first subsystem to design *Positive Electrode Estimator*, we treat anode state (x) contribution in terminal voltage V_t as an external uncertainty. Similarly, while using the second subsystem to design *Negative Electrode Estimator*, we treat cathode state (y) contribution in terminal voltage V_t as an external uncertainty. Note that these two subsystems are now separately observable from V_t under nominal (i.e. no uncertainty) condition.

A. Mathematical Form of the Algorithm

In this subsection, we discuss the mathematical forms of these aforementioned sub-estimators.

Positive Electrode Estimator: While designing the *Positive Electrode Estimator*, we treat the negative electrode quantities arising in the model as external uncertainty term. Such treatment allows us to decouple the design of two estimators in a separate manner. Consequently, from (1), we can write the positive electrode dynamics as:

$$\dot{y} = K_p I, \;\; \dot{K}_p = 0, \tag{4}$$

where $K_p = 1/Q_p$. Furthermore, we express the terminal voltage (3) as

$$V_t = c_1 y + f_1(y, I) + \eta_1, \tag{5}$$

where $c_1 y + f_1(y, I) = f_p(y) - IR_p(y)$ and $\eta_1 = -f_n(x) - IR_n(x)$. Note that the term $c_1 y$ represent the linear component of the OCP function $f_p(y)$ and the term $f_1(y, I)$ represents the rest of the nonlinearity of $f_p(y)$ as well as $-IR_p(y)$. Furthermore, as mentioned before, the term η_1 captures the effect of negative electrode related quantities in the dynamics and is treated as an external uncertainty. The dynamics of η_1 can be expressed as:

$$\dot{\eta}_1 = \alpha^T f(I), \tag{6}$$

where $\alpha = [\alpha_1, \alpha_2, \alpha_3, \alpha_4]^T$ and $f(I) = [I^2, I, \dot{I}, 1]^T$ with

$$\alpha_1 = \frac{\partial R_n}{\partial x}\frac{1}{Q_n}, \;\; \alpha_2 = \frac{\partial f_n}{\partial x}\frac{1}{Q_n} + \frac{\partial R_n}{\partial x}\frac{1}{Q_n}\dot{Q}_{SEI}, \tag{7}$$

$$\alpha_3 = -R_n(x), \;\; \alpha_4 = \frac{\partial f_n}{\partial x}\frac{1}{Q_n}\dot{Q}_{SEI}. \tag{8}$$

As will be seen later, expressing the terminal voltage in the form (5) will help in estimator design and convergence analysis.

Next, based on (4), (5), and (6), we choose the following structure for *Positive Electrode Estimator* dynamics:

$$\dot{\hat{y}} = \hat{K}_p I + L_1(V_t - \hat{V}_t),\ \dot{\hat{K}}_p = L_2(V_t - \hat{V}_t)I,$$
$$\dot{\hat{\eta}}_1 = \hat{\alpha}^T f(I),\ \dot{\hat{\alpha}} = L_3(V_t - \hat{V}_t)f(I), \tag{9}$$

where $\hat{V}_t = c_1\hat{y} + f_1(\hat{y}, I) + \hat{\eta}_1$ with $\hat{s}$ representing estimated value of s. The parameters L_1, L_2 and L_3 are the estimator gains, tuning parameters of the algorithm.

Negative Electrode Estimator: From (1), we can write the negative electrode dynamics as:

$$\dot{x} = K_n I + K_n K_2/z,\ \dot{z} = K_2/z,\ \dot{K}_n = 0, \tag{10}$$

where $K_n = -1/Q_n$, $z = Q_{SEI}$, and $K_2 = k_{SEI}^2/2$. Furthermore, we express the terminal voltage (3) as

$$V_t = c_2 x + f_2(x, I) + f_p(y) - IR_p(y), \tag{11}$$

where $c_2 x + f_2(x, I) = -f_n(x) - IR_n(x)$. The term $c_2 x$ represent the linear component of the OCP function $f_n(x)$ and the term $f_2(x, I)$ represents the rest of the nonlinearity of $f_n(x)$ as well as $-IR_n(x)$. Based on (10) and (11), we choose the following structure for *Negative Electrode Estimator* dynamics:

$$\dot{\hat{x}} = \hat{K}_n I + \hat{K}_n K_2/\hat{z} + L_4(V_t - \hat{V}_t),$$
$$\dot{\hat{z}} = K_2/\hat{z} + L_5(V_t - \hat{V}_t),\ \dot{\hat{K}}_n = L_6(V_t - \hat{V}_t)I, \tag{12}$$

where $\hat{V}_t = c_2\hat{x} + f_2(\hat{x}, I) + f_p(\bar{y}) - IR_p(\bar{y})$ with $\hat{s}$ representing estimated value of s and $\bar{y}$ is the estimated y from *Positive Electrode Estimator*. The parameters L_4, L_5 and L_6 are the estimator gains, tuning parameters of the algorithm.

Assumption 1. The parameters c_1, c_2, and $f_1(.)$ and $f_2(.)$ are chosen such that $f_1(.)$ and $f_2(.)$ exhibits Lipschitz continuity as follows:

$$\left|f_1\big(y^{(1)}, I\big) - f_1\big(y^{(2)}, I\big)\right| \le \gamma_1 \left|y^{(1)} - y^{(2)}\right|, \forall I,$$
$$\left|f_2\big(x^{(1)}, I\big) - f_2\big(x^{(2)}, I\big)\right| \le \gamma_2 \left|x^{(1)} - x^{(2)}\right|, \forall I, \tag{13}$$

where $y^{(1)}, y^{(2)} \in \mathcal{D}_y$, $x^{(1)}, x^{(2)} \in \mathcal{D}_x$ with $\mathcal{D}_y$ and $\mathcal{D}_x$ being the domains of x and y, respectively, and $\gamma_1, \gamma_2 > 0$ are Lipschitz constants. Furthermore, the constants γ_1 and γ_2 satisfy the following properties: $|c_1| > \gamma_1, |c_2| > \gamma_2$.

B. Stability Analysis of the Algorithm

Subtracting the estimator dynamics (9) from the plant dynamics (4)-(6), the estimation error dynamics of the *Positive Electrode Estimator* can be written as:

$$\dot{\tilde{y}} = \tilde{K}_p I - L_1\tilde{V}_t,\ \dot{\tilde{K}}_p = -L_2\tilde{V}_t I,$$
$$\dot{\tilde{\eta}}_1 = \tilde{\alpha}^T f(I),\ \dot{\tilde{\alpha}} = -L_3\tilde{V}_t f(I), \tag{14}$$

where $\tilde{s}$ represents the estimation error of s denoted by $\tilde{s} = s - \hat{s}$, and $\tilde{V}_t = c_1\tilde{y} + \tilde{f}_1 + \tilde{\eta}_1$ with $\tilde{f}_1 = f_1(y, I) - f_1(\hat{y}, I)$. Similarly, subtracting the estimator dynamics (12) from the plant dynamics (10)-(11), the estimation error dynamics of the *Negative Electrode Estimator* can be written as:

$$\dot{\tilde{x}} = \tilde{K}_n I + K_2\frac{\tilde{K}_n}{z} - \frac{K_2\hat{K}_n}{z\hat{z}}\tilde{z} - L_4\tilde{V}_t,$$
$$\dot{\tilde{z}} = K_2\Big(\frac{1}{z} - \frac{1}{\hat{z}}\Big) - L_5\tilde{V}_t,\ \dot{\tilde{K}}_n = -L_6\tilde{V}_t I, \tag{15}$$

where $\tilde{V}_t = c_2\tilde{x} + \tilde{f}_2 + \omega$ with $\tilde{f}_2 = f_2(x, I) - f_2(\hat{x}, I)$. The term ω represents error arising from the difference between y and $\bar{y}$, that is, the estimation inaccuracies of *Positive Electrode Estimator*. Based on these error dynamics (14) and (15) and the following framework presented in [4], the following propositions illustrate the stability properties of the estimation algorithm.

Proposition 1. *(Stability of the Positive Electrode Estimator Error Dynamics) Consider the estimation error dynamics* (14)*. If Assumption 1 is true, and the estimator gains L_1, L_2 and L_3 are chosen such that the following conditions are satisfied: $L_2 = c_1/\theta_1, L_3 = \theta_2$ and $\mathbb{X} \le 0$ where $\theta_1, \theta_2 > 0$ are arbitrary positive constants and*

$$\mathbb{X} = \begin{bmatrix} x_{11} & x_{12} & x_{13} & x_{14} \\ 0 & 0 & 0 & x_{24} \\ 0 & 0 & 0 & 0 \\ 0 & 0 & 0 & 0 \end{bmatrix} \tag{16}$$

with $x_{11} = -L_1\theta_1 c_1 + |L_1|\,\theta_1\gamma_1$, $x_{12} = |L_1|\,\theta_1$, $x_{13} = L_3\|f(I)\|(c_1 + \gamma_1)$, $x_{14} = L_2\gamma_1|I|$, $x_{24} = L_2|I|$; then the estimation errors $|\tilde{y}|, \|\tilde{\alpha}\|, |\tilde{\eta}_1|$ and $|\tilde{K}_p|$ will remain uniformly bounded as $t \to \infty$.

Proof. We consider the following positive definite Lyapunov function candidate:

$$W_1 = \frac{\theta_1}{2}\tilde{y}^2 + \frac{1}{2}\tilde{K}_p^2 + \frac{1}{2}\tilde{\alpha}^T\tilde{\alpha} + \frac{\theta_2}{2}\tilde{\eta}_1^2 \tag{17}$$

with $\theta_1 > 0$ and $\theta_2 > 0$. Differentiating W_1 with respect to time and subsequently, using (14), we get:

$$\dot{W}_1 = \theta_1\tilde{y}\tilde{K}_p I - L_1\theta_1\tilde{y}\tilde{V}_t - \tilde{K}_p L_2\tilde{V}_t I + \theta_2\tilde{\eta}_1\tilde{\alpha}^T f(I) - \tilde{\alpha}^T L_3\tilde{V}_t f(I). \tag{18}$$

Next, (i) using the expression $\tilde{V}_t = c_1\tilde{y} + \tilde{f}_1 + \tilde{\eta}_1$ where $\tilde{f}_1 = f_1(y, I) - f_1(\hat{y}, I)$, (ii) considering the fact $\left|\tilde{f}_1\right| \le \gamma_1\,|\tilde{y}|$ from Assumption 1 and the inequality $m_1^T m_2 \le \|m_1\|\,\|m_2\|$, and (iii) applying $L_2 = c_1/\theta_1$ and $L_3 = \theta_2$, we write (18) as:

$$\dot{W}_1 \le |\tilde{y}|^2\{-L_1\theta_1 c_1 + |L_1|\,\theta_1\gamma_1\} + |\tilde{y}|\,|\tilde{\eta}_1|\,L_1\theta_1 + |\tilde{y}|\,\|\tilde{\alpha}\|\{L_3\|f(I)\|(|c_1| + |\gamma_1|)\} + \left|\tilde{K}_p\right||\tilde{y}|\,\{L_2\gamma_1\,|I|\} + \left|\tilde{K}_p\right||\tilde{\eta}_1|\,\{L_2\,|I|\}, \tag{19}$$

which we can further re-write in vector-matrix form as $\dot{W}_1 \le \beta^T\mathbb{X}\beta$ where $\beta = [|\tilde{y}|, |\tilde{\eta}_1|, |\tilde{\alpha}|, |\tilde{K}_p|]^T$ and $\mathbb{X}$ is given in (16). Note that by choice of L_1, we can ensure $x_{11} < 0$ and hence, $\mathbb{X} \le 0$. Consequently, we can conclude that $\dot{W}_1 \le 0$. Negative semidefiniteness of $\dot{W}_1$ confirms that the estimation errors $|\tilde{y}|$, $|\tilde{\eta}_1|$, $|\tilde{\alpha}|$, and $|\tilde{K}_p|$ will remain bounded as $t \to \infty$. □

Proposition 2. *(Stability of the Negative Electrode Estimator Error Dynamics) Consider the estimation error dynamics* (15)*. If Assumption 1 is true and* $\omega = 0$*, and the estimator gains* L_4, L_5, L_6 *are chosen such that the following conditions are satisfied:* $L_5 > 0, L_6 = \theta_3/c_2$ *and* $\mathbb{Y} \leq 0$ *where* θ_3 *is an arbitrary positive constant, and*

$$\mathbb{Y} = \begin{bmatrix} y_{11} & y_{12} & y_{13} \\ 0 & y_{22} & 0 \\ 0 & 0 & 0 \end{bmatrix} \tag{20}$$

with $y_{11} = \theta_3(-L_4c_2 + |L_4|\gamma_2)$, $y_{12} = L_5(|c_2| + \gamma_2) + \theta_3 \left|\frac{K_2\tilde{K}_n}{z\hat{z}}\right|$, $y_{13} = |L_6|\gamma_2|I| + \theta_3\frac{K_2}{z}$ *and* $y_{22} = -\frac{K_2}{z\hat{z}}$*, then the estimation errors* $|\tilde{x}|$, $|\tilde{z}|$ *and* $|\tilde{K}_n|$ *will remain uniformly bounded as* $t \to \infty$.

Proof. We consider the following positive Lyapunov function candidate

$$W_2 = \frac{\theta_3}{2}\tilde{x}^2 + \frac{1}{2}\tilde{z}^2 + \frac{1}{2}\tilde{K}_n^2, \tag{21}$$

where $\theta_3 > 0$. Next, (i) differentiating W_2 with respect to time and using the expression (15), (ii) considering the fact $|\tilde{f}_2| \leq \gamma_2|\tilde{x}|$ from Assumption 1 and the inequality $n_1n_2 \leq |n_1|\,|n_2|$, we get:

$$\begin{aligned} \dot{W}_2 &\leq \theta_3\tilde{x}\tilde{K}_nI - L_6c_2\tilde{K}_n\tilde{x}I - L_4\theta_3c_2|\tilde{x}|^2 + \theta_3|L_4|\gamma_2|\tilde{x}|^2 \\ &+ L_5|c_2||\tilde{x}||\tilde{z}| + L_5\gamma_2|\tilde{x}||\tilde{z}| - \frac{K_2}{z\hat{z}}|\tilde{z}|^2 + \gamma_2|L_6||\tilde{K}_n||\tilde{x}||I| \\ &\theta_3\frac{K_2}{z}\left|\tilde{K}_n\right||\tilde{x}| + \theta_3\left|\frac{K_2\hat{K}_n}{z\hat{z}}\right||\tilde{z}|\,|\tilde{x}|\,. \end{aligned} \tag{22}$$

With the choice of $L_6 = \theta_3/c_2$, we can write $\dot{W}_2$ expression in the following vector-matrix form: $\dot{W}_2 \leq \lambda^T\mathbb{Y}\lambda$ where $\lambda = [|\tilde{x}|, |\tilde{z}|, |\tilde{K}_n|]^T$ and $\mathbb{Y}$ is given in (20). By choice of L_4 we can ensure $-L_4\theta_3c_2 + |L_4|\theta_3\gamma_2 < 0$, and we know $K_2, z, \hat{z} > 0$ from the physical properties of the battery model. Hence, we can ensure $\mathbb{Y} \leq 0$ which in turn confirms that the errors $|\tilde{x}|, |\tilde{z}|$ and $|\tilde{K}_n|$ will remain bounded as $t \to \infty$. □

IV. EXPERIMENTAL IDENTIFICATION OF BATTERY MODEL

In this section, we discuss the experimental identification of the battery model discussed in Section II. The pouch type battery cell under consideration has the following characteristics: cathode material NMC532, anode material Silicon/Graphite/Binder with 15/73/12 weight %, total cell capacity 400 mAh, maximum voltage 4.1 V, and minimum voltage 3.0 V. Cells were fabricated by Argonne National Lab Cell Analysis Modeling Prototype facility. In the experimental setup, reference electrode method has been used to collect anode potential data along with cell terminal voltage data. Two separate channels in the Arbin BT2000 battery cycler have been used to measure the anode potential and terminal voltage with sample time of 20 seconds and 10 seconds, respectively. The OCP functions $f_p(.)$ and $f_n(.)$ were measured and identified at a constant current rate of $C/10$, as such smaller current better capture the *equilibrium* behavior of the battery cell and electrodes. The identified OCP functions are shown in Fig. 2 and Fig. 3. The stoichiometry points corresponding to 0% full cell SOC are $x_0 = 0.05, y_0 = 0.88$ and the points corresponding to 100% full cell SOC are $x_{100} = 0.7, y_{100} = 0.4$.

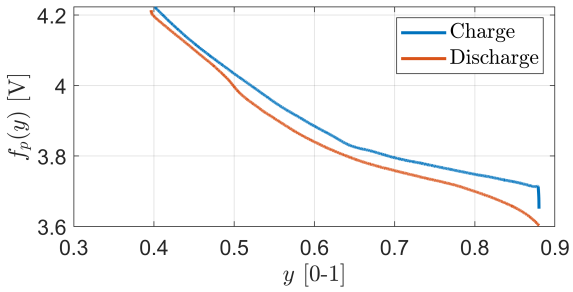

Fig. 2. Identified positive electrode OCP function.

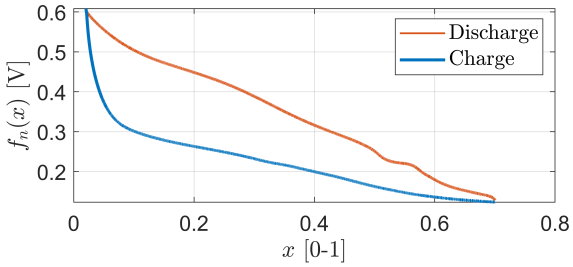

Fig. 3. Identified negative electrode OCP function.

After identifying the OCP functions, we focus on identifying the rest of the model parameters: electrode capacities Q_p and Q_n, SEI parameter k_{SEI}, and electrode resistances R_p and R_n. In order to capture the nonlinear dependencies of electrode resistances on electrode SOCs, we have assumed the following polynomial form of the resistance functions:

$$\begin{aligned} &\text{Charge: } R_p(y) = \sum_{i=0}^{n_c} P_{ci}y^i, \text{Discharge: } R_p(y) = \sum_{i=0}^{n_d} P_{di}y^i \\ &\text{Charge: } R_n(x) = \sum_{i=0}^{m_c} N_{ci}x^i, \text{Discharge: } R_n(x) = \sum_{i=0}^{m_d} N_{di}x^i \end{aligned} \tag{23}$$

where P_{ci}, P_{di}, N_{ci}, and N_{di} are the coefficients of the polynomial functions. We have used $C/3$ constant current data to identify the aforementioned parameters. First, we have computed individual electrode potential data from cell terminal voltage and anode potential measurements. Subsequently, we have solved the following optimization problems:

$$\min_{\vartheta_n} RMS(V_{ae} - V_{am}(\vartheta_n)),\ \min_{\vartheta_p} RMS(V_{ce} - V_{cm}(\vartheta_p))$$

with respect to dynamic constraints (1)-(2) and,

$$\vartheta_{p_{min}} \leq \vartheta_p \leq \vartheta_{p_{max}}, \vartheta_{n_{min}} \leq \vartheta_n \leq \vartheta_{n_{max}}, \tag{24}$$

where $\vartheta_n = \{Q_n, k_{SEI}, Q_{SEI}(0), N_{ci}, N_{di}\}$ and $\vartheta_p = \{Q_p, P_{ci}, P_{di}\}$; $RMS(.)$ indicates the root mean square operator; $\vartheta_{p_{max}}, \vartheta_{n_{max}}$ and $\vartheta_{p_{min}}, \vartheta_{n_{min}}$ are the upper and lower bounds of the parameters; V_{ae} and V_{am} are the anode

potential data from experiments and model, respectively; V_{ce} and V_{cm} are the cathode potential data from experiments and model, respectively.

We have solved the optimization problem (24) using Genetic Algorithm (GA) framework. The identification process resulted in 4.2 mV and 8.8 mV of RMS errors for cathode and anode models, respectively. The identified parameters are given in Table I.

TABLE I
IDENTIFIED PARAMETERS

Parameters	Values	Parameters	Values
$Q_{SEI}(0)$	5.2391×10^{-8} Ah	Q_p	0.74 Ah
k_{SEI}	7.2802×10^{-5} A$\sqrt{s}$	Q_n	0.57 Ah
P_{c0}	-2.528	P_{d0}	4.54
P_{c1}	13.44	P_{d1}	-30.31
P_{c2}	-21.33	P_{d2}	77.44
P_{c3}	11.19	P_{d3}	-88.96
P_{c4}	0	P_{d4}	38.85
N_{d0}	0.6295	N_{d3}	-168.1
N_{d1}	-7.717	N_{d4}	268.4
N_{d2}	51.66	N_{d5}	-186.5
N_{ci}	0, $\forall i$	N_{d6}	32

V. ESTIMATION RESULTS AND DISCUSSION

In this section, we present simulation case studies in MATLAB/Simulink platform, based on the identified model in the previous section. As discussed in the formulation of the estimation algorithm, we are interested in estimating x, y, Q_n, Q_p and Q_{SEI}. In the estimation algorithm, the estimated variables are initialized with incorrect values to evaluate their convergence. Specifically, we have used 10% initial error in our case studies. Next, we perform the following case studies.

A. Case Study 1: Constant Current Charging Scenario

In the first case study, we have considered a constant current scenario where the battery cell is being charged at $C/3$ rate. The estimation results for positive and negative stoichiometries and capacities (y, x, Q_p, Q_n) are illustrated in Fig. 4 and Fig. 5. Furthermore, Q_{SEI} estimation is shown in Fig. 6. It can be seen that all the estimated variables converged close to the true variables starting from incorrect initial condition. The *steady-state errors* for the x and y estimation are 0.7% and 0.3%, and for Q_n and Q_p estimation are 0.03% and 2.2%, respectively. The *convergence times* for the x, y, Q_n, Q_p are $3.18, 24.6, 5.46, 24.6$ minutes, respectively.

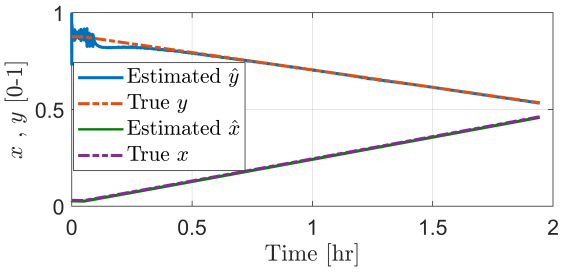

Fig. 4. Stoichiometry estimation results under $C/3$ constant charging rate.

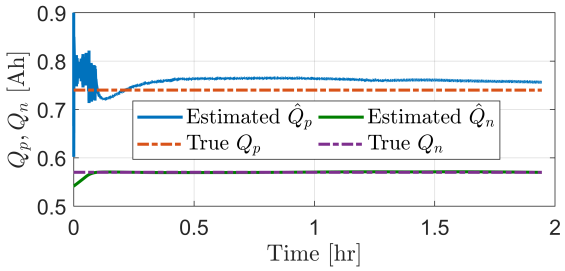

Fig. 5. Capacity estimation results under $C/3$ constant charging rate.

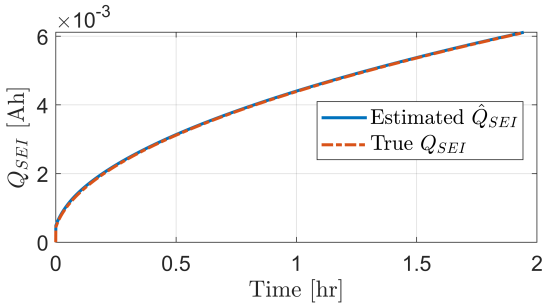

Fig. 6. SEI growth estimation result under $C/3$ constant charging rate.

B. Case Study 2: Dynamic Current Discharging Scenario

In the second case study, we have subjected the battery cell under modified US06 type dynamic discharge current profile as shown in Fig 7. The estimation results for the stoichiometries and capacities (y, x, Q_p, Q_n) are shown in Fig. 8 and Fig. 9. The Q_{SEI} estimation is shown in Fig. 10. From the results, it can be seen that the estimated variables converged to their true values with the *steady-state errors* of 2.9%, 0.8%, 0.7%, and 1.86% for the variables x, y, Q_n and Q_p, respectively. The *convergence times* for the x, y, Q_n, Q_p estimation are 60, 36, 34.2 and 38.4 minutes, respectively.

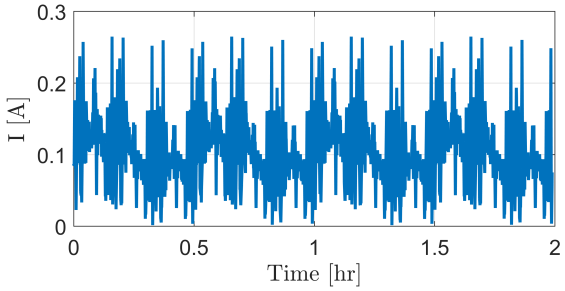

Fig. 7. Dynamic discharge current profile.

C. Case Study 3: Robustness with Respect to Uncertain SEI Parameter

In this case study, the robustness of estimation algorithm is studied with respect to SEI model parameter k_{SEI}. We have applied the same current profile as in case study 1. The estimation results for Q_n and Q_{SEI} are shown in Fig. 11 under different levels of uncertainty. From Fig. 11, we can conclude that the estimation error for Q_n and Q_{SEI} stay within a tolerable range under 5% uncertainty in k_{SEI}. However, the estimation performance reduces notably beyond 10% uncertain k_{SEI}.

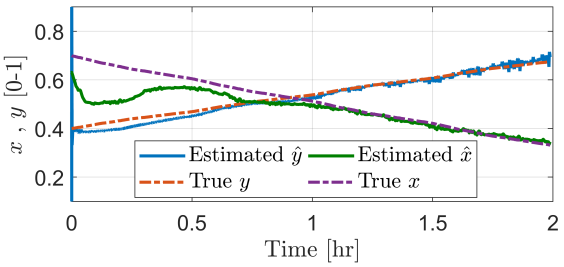

Fig. 8. Stoichiometry estimation results under dynamic discharge current with 10% initial estimation error for all variables.

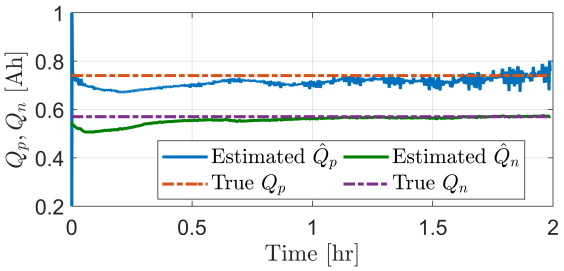

Fig. 9. Capacity estimation results under dynamic discharge current with initial estimation errors of 10% and 5% for Q_p and Q_n, respectively.

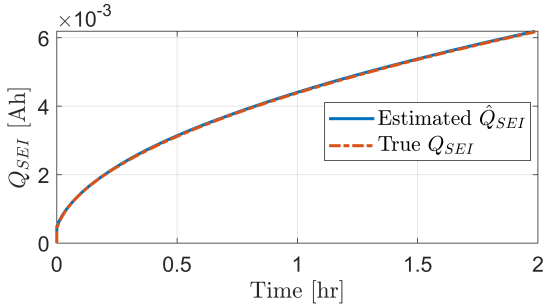

Fig. 10. SEI growth estimation results under dynamic discharge current with initial estimation error of 10%.

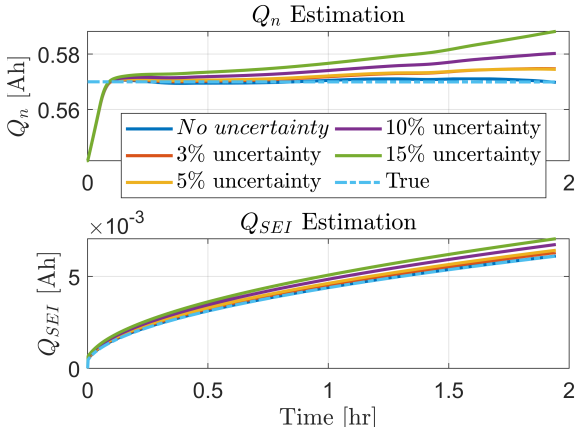

Fig. 11. Negative electrode capacity and SEI growth estimation under different levels of uncertainties in k_{SEI}.

VI. CONCLUSIONS

We have designed an online estimation algorithm to estimate available charge and capacity of individual electrodes in a battery cell. This estimation framework addresses the critical issue of battery observability where individual electrode states are weakly observable from terminal voltage measurement. The mathematical properties of the proposed estimation algorithm are analyzed via Lyapunov's stability theory. An experimentally identified electrode-level battery model with nonlinear OCP functions, electrode resistances and SEI dynamics is used to perform simulation studies to illustrate the effectiveness of the proposed approach. As future work, we plan to validate the proposed approach with experimental data.

ACKNOWLEDGMENT

This work was authored in part by Alliance for Sustainable Energy, LLC, the manager and operator of the National Renewable Energy Laboratory for the U.S. Department of Energy (DOE) under Contract No. DE-AC36-08GO28308. Funding is provided in part by the National Renewable Energy Laboratory via subcontract no. XCE-9-92129-01 (under prime contract no. DE-AC36-08GO28308), and National Science Foundation under award no. 1908560. The views expressed in the article do not necessarily represent the views of the DOE or the U.S. Government. The U.S. Government retains and the publisher, by accepting the article for publication, acknowledges that the U.S. Government retains a nonexclusive, paid-up, irrevocable, worldwide license to publish or reproduce the published form of this work, or allow others to do so, for U.S. Government purposes.

REFERENCES

[1] D. Di Domenico, A. Stefanopoulou, and G. Fiengo, "Lithium-ion battery state of charge and critical surface charge estimation using an electrochemical model-based extended kalman filter," *Journal of dynamic systems, measurement, and control*, vol. 132, no. 6, p. 061302, 2010.

[2] S. Dey, B. Ayalew, and P. Pisu, "Nonlinear robust observers for state-of-charge estimation of lithium-ion cells based on a reduced electrochemical model," *IEEE Transactions on Control Systems Technology*, vol. 23, no. 5, pp. 1935–1942, 2015.

[3] A. Allam and S. Onori, "An interconnected observer for concurrent estimation of bulk and surface concentration in the cathode and anode of a lithium-ion battery," *IEEE Transactions on Industrial Electronics*, vol. 65, no. 9, pp. 7311–7321, 2018.

[4] S. Dey, Y. Shi, K. Smith, A. Colclasure, and X. Li, "From battery cell to electrodes: Real-time estimation of charge and health of individual battery electrodes," *IEEE Transactions on Industrial Electronics*, 2019.

[5] S. Dey and B. Ayalew, "Real-time estimation of lithium-ion concentration in both electrodes of a lithium-ion battery cell utilizing electrochemical–thermal coupling," *Journal of Dynamic Systems, Measurement, and Control*, vol. 139, no. 3, p. 031007, 2017.

[6] S. J. Moura, F. B. Argomedo, R. Klein, A. Mirtabatabaei, and M. Krstic, "Battery state estimation for a single particle model with electrolyte dynamics," *IEEE Transactions on Control Systems Technology*, vol. 25, no. 2, pp. 453–468, 2016.

[7] A. Bartlett, J. Marcicki, S. Onori, G. Rizzoni, X. G. Yang, and T. Miller, "Electrochemical model-based state of charge and capacity estimation for a composite electrode lithium-ion battery," *IEEE Transactions on control systems technology*, vol. 24, no. 2, pp. 384–399, 2015.

[8] P. Mohtat, S. Lee, J. B. Siegel, and A. G. Stefanopoulou, "Towards better estimability of electrode-specific state of health: Decoding the cell expansion," *Journal of Power Sources*, vol. 427, pp. 101–111, 2019.